RSC Advances

ROYAL SOCIETY OF CHEMISTRY

www.rsc.org/advances

RSC Advances

PAPER

Microfluidic self-aspiration sonic-spray ionization chip with single and dual ionization channels for mass spectrometry

Received 00th January 20xx,
Accepted 00th January 20xx

DOI: 10.1039/x0xx00000x

www.rsc.org/

Cilong Yu,[a,c] Xiang Qian,[a,*] Yan Chen,[b] Quan Yu,[a] Kai Ni[a] and Xiaohao Wang[a,c,d*]

The coupling of microfluidic chip-based ionization to mass spectrometer (MS) has recently gained considerable attention in the mass spectrometry community. In consideration of the miniaturization, integration, and universal disadvantages of microfluidic chip-based ionization coupled with MS, this study proposed a novel microfluidic self-aspiration sonic-spray ionization chip. The proposed ionization chip was fabricated using three-layer soft lithography technology without the need to fabricate the spraying tips. Simulations were performed to validate and optimize the microfluidic structure for self-aspiration. Corresponding experiment results were obtained by characterizing and comparing the MS signals of different microfluidic chip structures coupled with an ion-trap MS. MS signals of different gases for sonic-spray ionization for different liquid samples were also compared. Results indicated that the proposed microfluidic chip can implement the ionization of liquid samples depending simply on the gas applied on the sheath flow channel with much lower gas pressure. Moreover, dual-channel self-aspiration sonic-spray ionization chip was implemented, which might realize internal calibration for MS. We premilinarily proved the intensity enhancement by applying the same sample in both channels and reduced the ion suppression by applying different samples in different channels. This microfluidic chip significantly improved the integration of ionization and simplified the operation of such device, making it particularly suitable for coupling with portable MS in the future.

Introduction

Mass spectrometry plays an essential role in analytical fields. Miniaturization and simplification are two of the developing directions of mass spectrometer (MS).[1, 2] Ionization techniques performed from "inhospitable" high-vacuum environments to atmospheric pressure outside the MS strongly simplify MS analysis.[3] The majority of atmospheric pressure ionizations, such as electrospray ionization (ESI),[4] desorption ESI,[5] direct analysis in real time (DART),[6] low-temperature plasma (LTP),[7] and easy ambient sonic-spray ionization (EASI),[8] consist of nebulizer gas. Pneumatic nebulization of a charged liquid stream helps generate stable signal intensity over a broad flow rate range; the technique also provides a response dynamic range of 10^3–10^4 while maintaining relative insensitivity to changes in voltage, mobile phase composition, sprayer position, and electrode dimensions.[9] Furthermore, pneumatic nebulization is indispensable in various ambient desorption ionizations, such as Venturi EASI (V-EASI), in which the charges and even driving force of liquid are dependent only on high-velocity gas flow.[3] V-EASI, which is based on sonic-spray ionization (SSI),[10] is solely dependent on high-velocity gas flow and requires no assistance from high voltages, heating, and even pump for samples.[3] The characteristics of the SSI, with and without electricity, have been studied comprehensively by Cooks *et al.*[11-13] Subsequently, Eberlin *et al.* revisited this technology by studying the desorption function[8, 14, 15] and various applications of the SSI.[16-19] Currently, considerable research is focused mainly on improving sensitivity and alleviating the ion suppression effect of the SSI.[20, 21] Meanwhile, most microfluidic-based ionization design lacks gas atomizing, desorption functions and many other ionization methods. Several research groups have comprehensively reviewed the coupling of microfluidic-based ionization to MS.[22-25] Microfluidic chip-based ESI sources are generally divided into three types. The first type is monolithic ionization, which involves direct spraying from the edge of a microfluidic chip, and was earlier reported by Karger *et al.*[26] and Ramsey *et al.*[27] Such ionization chips encountered liquid-spreading problems along the edge of the microfluidic chip, and thus led to the formation of a large Taylor cone. Tapered fused-silica capillaries, which served as electrospray tips, were inserted into the end of the microfluidic channels to overcome this problem.[28] However, the fabrication process was difficult. Large dead volumes were generated at the interfaces between the capillaries and the micro-channels, thus causing a possible degradation of the electrospray performance. In recent years,

[a] Division of Advanced Manufacturing, Graduate School at Shenzhen, Tsinghua University, Shenzhen, 518055, China. E-mail: qian.xiang@sz.tsinghua.edu.cn (X.Q.); Tel: +86-755-2603-6755 (X.Q.).
[b] Shenzhen Institutes of Advanced Technology, Chinese Academy of Sciences, Shenzhen 518055, China.
[c] The State Key Laboratory of Precision Measurement Technology and Instruments, Tsinghua University, Beijing 100084, China. E-mail: wang.xiaohao@sz.tsinghua.edu.cn (X.W.); Tel: +86-755-2603-6213 (X.W.).
[d] The Research Institute of Tsinghua University in Shenzhen, Shenzhen 518057, China.

an increasing number of research efforts have adopted the design of integrated nozzles in microfluidic chip during the fabrication process.[29] This approach undoubtedly possesses distinct advantages compared with previous methods. In addition, the integrated nozzle was developed from one nozzle to multi-nozzles for high-throughput analysis.[30, 31] However, forming an excellent electrospray nozzle integrated on the microfluidic chip is difficult, because the polydimethylsiloxane (PDMS) is soft and the tip is very small to be cut at the two sides of the micro-channel front end.[32] Thus, these disadvantages significantly weaken the applications of microfluidic-based ionization coupled with MS. For example, digital microfluidic (DMF) based on the electro-wetting on dielectric phenomenon is still difficult to combine with on-line MS detection for numerous analytical laboratories. In a latest study, a macrostructure V-EASI connecting to an open DMF microfluidic chip was applied to realize coupling with MS.[33] Therefore, if the macrostructure V-EASI can be realized in microfluidic chip, then DMF with other functions might be facile to couple with MS in a single microfluidic chip.

Our previous work successfully introduced the gas phase sheath flow into the microfluidic chip and realized electro-flow focusing ionization[34] with the following aims: to improve the coupling of microfluidic chip ionization to MS, enrich the diversities of microfluidic chip ionization spray forms, and settle the manufacture problems of the integrated nozzle on microfluidic chip. On the basis of the preceding effort, the present study proposed a novel microfluidic chip structure that can implement self-aspiration samples by using the negative pressure generated by the high gas flow velocity. Moreover, this microfluidic chip can realize sample ionization without high voltage under atmospheric pressure. The proposed microfluidic self-aspiration SSI chip was fabricated using three-layer soft lithography technology. Simulations were conducted to validate and optimize the microfluidic structure for self-aspiration, and the experiment results of different chip structures were compared. Three gases, including helium, nitrogen, and argon, were likewise applied for SSI with various samples. The MS signals of a home-made macro self-pumping SSI and the proposed ionization chip were compared. The results indicated that the proposed ionization chip can obtain stable MS signals without high voltage and sample injection apparatus. This ionization chip also required much lower gas pressure compared with the macro SSI system. Moreover, because of the severe interference among the electric fields of the adjacent sprayers, microfluidic chip based dual-sprayers failed to generate signals of the analyte and the reference compounds simultaneously, as Ramsey *et al*.[35] reported currently. Thus, dual-channel self-aspiration sonic-spray ionization chip without high voltage was proposed, which might realize internal calibration for MS. We preliminarily proved the intensity enhancement by applying the same sample in both channels and reduced the ion suppression by applying different samples in different channels. All these characteristics allowed easy on-chip parallel ionization, integration with other pre-treatment module, and coupling with the portable and miniature MS.

Materials and Methods

Materials and Equipment

HPLC-grade methanol and acetic acid were purchased from Merck KGaA (Darmstadt, Germany). PDMS elastomer base and curing agent (Sylgard 184) were purchased from Dow Corning (Midland, MI, USA). SU-8 photoresist was obtained from Microchem Co. (Naton, MA, USA). All solvents and samples used in this study were obtained from commercial sources. Gas was supplied to the microfluidic chip through short stainless steel tubes embedded in the reservoir using an Electro-Pneumatic Regulator ITV 2050-312N (SMC Co., Tokyo, Japan). Liquid samples were introduced into a 200 µL tip (Type A, Gelloading) by a transfer liquid gun, the tip was inserted in the liquid reservoir of the microfluidic chip. A high-speed camera (ORCA-flash, Hamamatsu) mounted on an inverted optical microscope (Eclipse TE 2000-U, Nikon) was used to observe the experiments. A thermo LCQ MS (Thermo Fisher Scientific Inc., Waltham, MA, USA) was coupled with the microfluidic chip placed on a multi-dimensional manipulator. The MS data were collected by a computer.

Microfluidic Chip Design

A three layers design was applied in this novel microfluidic self-aspiration SSI chip, which implemented automatic sampling and avoided the problem of manufacturing the spraying tip. In most cases, the top and bottom halves of the nozzle tend to separate at the tip, which seriously affects the spray effect. [32] Moreover, care must be taken when cutting along the edge of the nozzle outlet to form an excellent spray tip. The proposed structure and corresponding fabrication process successfully avoided these drawbacks. Similar to coaxial capillary tubes, the gas channel in this microfluidic chip was distributed in parallel at the two sides of the liquid channel front end, as shown in Fig. 1. The liquid channel was recessed inside the nozzle outlet, as shown in Fig. 2b. Under such conditions, high gas flow rate generated negative pressure at the liquid channel front end, which aspirated the liquid samples out of the channel and sprayed them out automatically, as proved by simulation in Fig. 3 and Fig. 4. The microfluidic chip was designed by AutoCAD (Autodesk, Inc., San Rafael, CA, USA). The photo masks and nozzle size of the microfluidic chip are presented in Fig. 1. Three

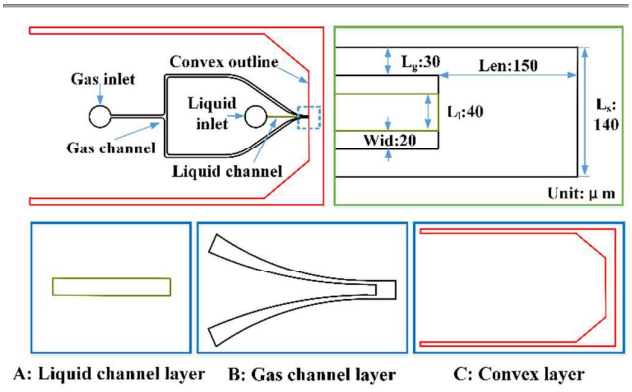

Fig. 1 Photo masks and nozzle size of the microfluidic chip. Photo masks of A, B, and C show the liquid channel layer, gas channel layer, and convex layer, respectively.

photo masks, including liquid channel layer, gas channel layer, and convex layer (as illustrated in Figs. 1 A, B, and C, respectively), were manufactured by Qingyi Precision Mask Making Co., Ltd. (Shenzhen, China). The liquid channel layer and gas channel layer were used to form a liquid channel and a gas channel, respectively. To ensure the nozzle was solely shaped by the lithographically created microstructures and would not be touched by the razor blade,[36] the convex layer was applied to form the cutting outline (as indicated by dashed lines in Fig. 2b) for the razor blade to cut off the excess PDMS at the nozzle front end. The heights of the liquid and air channel were approximately 25 and 100 µm respectively. In the dual-channel microfluidic chip, the three gas channels and two liquid channels was arranged in the staggered distribution, that there were gas channels at the two sides of each liquid channel and the two liquid channels shared the middle gas channel. The distance between liquid channel front end and nozzle outlet, defined as the parameter *Len*, was 100 µm in Fig. 1. The wall thickness between gas channel and liquid channel, defined as the parameter *Wid*, was 40 µm in Fig. 1.

Fabrication of the Microfluidic Chip

The microfluidic chip was fabricated using standard multilayer soft lithography techniques with the following steps:[34, 37, 38]

(1). A 3-inch silicon wafer template was treated in oxygen plasma (PDC-M, Chengdu Mingheng Science & Technology Co., Ltd, Chengdu, China) to prevent SU-8 photoresist from spalling; (2). The negative photoresist (SU-8 2025) was then poured on the silicon wafer for spinning and soft-baking;

(3). The photoresist was exposed via photo mask A. This photo mask served as the liquid channel layer and provided an orifice and a channel for the liquid samples;

(4). Putting this SU-8 master mold on thermostatic platform for post-baking;

(5). The second layer of negative photoresist (SU-8 2100) was applied at the top of the liquid channel layer for spinning and soft-baking, without developing uncross-linked photoresist;

(6). Photo mask B, which was aligned with the liquid channel layer by a UV aligner, was placed on the second layer photoresist for exposure. This second layer served as the gas channel layer with the channels and orifice for the gas flow;

(7). Putting this SU-8 master mold on thermostatic platform for post-baking again;

(8). The third layer of negative photoresist (SU-8 2100) was applied at the top of the gas channel layer for spinning and soft-baking. The development of uncross-linked photoresist was also avoided;

(9). Photo mask C, which was aligned with the gas channel layer by a UV aligner, was placed on the third layer photoresist for exposure. This third layer served as the convex layer with the convex plate edge for cutting;

(10). Putting this SU-8 master mold on thermostatic platform for post-baking;

(11). The SU-8 photoresist layers were developed in propylene glycol methyl ether acetate;

(12). Then, this SU-8 master mold was placed on the thermostatic platform for hard-baking.

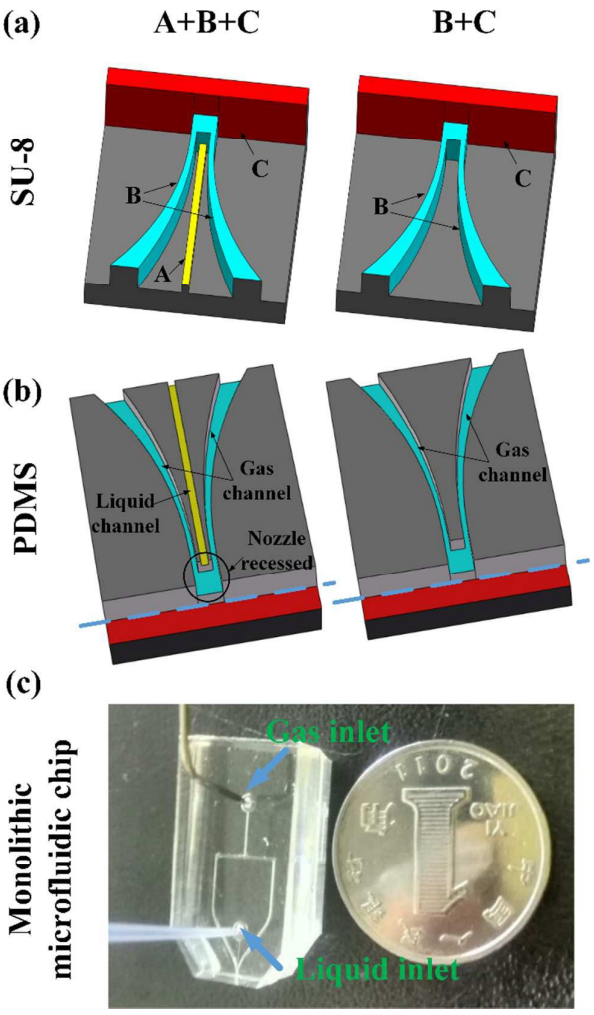

Fig. 2 (a) Top and the bottom SU-8 master molds; (b) Top and the bottom structures of the PDMS layers, where the dashed lines are the cutting outlines formed by the convex layer; (c) Monolithic microfluidic chip.

This SU-8 master mold served as the top layer of our micro-channel structure. Another SU-8 master mold with patterns of photo masks B and C only was prepared on another 3-inch silicon wafer template for the bottom PDMS micro-channel half-devices. This SU-8 master mold only had gas channel and convex layers; hence, the fabrication process was step (5) – (12). The final structures of the SU-8 master molds are illustrated in Fig. 2a.

The fabrication procedure of microfluidic chip using PDMS was as follows:

(1). The SU-8 master molds were modified with vapor-phase chlorotrimethylsilane to assist the release of PDMS membranes;
(2). PDMS base monomer and curing agent were mixed at 10:1 and 5:1 weight ratios, and then the mixtures were poured on the top and bottom SU-8 master molds;
(3). The two half-pieces were degassed under vacuum for about 20 minutes;
(4). The two half-pieces were then cured in an oven at 80 °C for 0.5 h;
(5). Two PDMS slabs were peeled off from the two master molds, and the inlet holes were drilled at the top by using a punch (tip diameter of 0.75 mm);
(6). Cutting off the excess PDMS. In general, considerable attention should be paid to remove the excess PDMS along the nozzle tips with a razor blade. However, in this study, a razor blade was only required to cut off the excess PDMS along the convex plate edge, denoted as the area below the dashed lines shown in Fig. 2b;
(7). Both PDMS slabs were treated in oxygen plasma (PDC-M, Chengdu Mingheng Science & Technology Co., Ltd, Chengdu, China), and then bonded together by using an xyz-manipulator (Beijing Optical Century Instrument Co., Ltd., Beijing, China);
(8). the PDMS microfluidic chip was cured at 80 °C for 48 h to enhance the bonding strength and eliminate the MS background from PDMS.
The final monolithic microfluidic chip is shown in Fig. 2c.

Results and Discussions

Simulation Analysis of Microfluidic Chip Structure

Computational fluid dynamic (CFD) simulation is a powerful tool for optimizing microfluidic chip designs.[36, 39-41] In this study, the negative pressure generated by high gas flow rate at the liquid channel front end was analyzed by using two-dimensional ANSYS FLUENT simulation. The proposed microfluidic chip structure was symmetrical, and thus, a half structure was imported into the ICEM CFD 14.5 in ANSYS from AutoCAD. This approach reduced the amount of necessary finite elements, economized the calculation time, and lowered the computer requirements. After dividing the finite elements, this model was imported into ANSYS FLUENT for calculation. Such gas flow CFD simulation was important to validate and optimize the microfluidic chip structure. In this model, only the gas channel inlet was set as the pressure inlet. The liquid channel inlet and nozzle outlet were all set as pressure outlet, and all cell zones were for gas flow. Considering the high flow rate, the k-epsilon (2-eqn) model was chosen and the gas was assumed to be compressible. For the sake of precision, second-order accuracy was set in the solution methods.
As shown in Fig. 3a, when the gas channel inlet was set as 0.3 MPa, negative pressure was generated at the liquid channel front end and the absolute pressure value reached 10^4 Pa. This pressure drop between the liquid channel front end and liquid channel inlet produced a driving force, which was large enough to drive the liquid to spray out from the liquid channel inlet. Therefore, this structure could realize self-aspiration by depending simply on gas flow. Moreover, the highest gas velocity was approximately 486 m/s, as shown in the velocity–magnitude nephogram, this was similar to the result of the paper.[41] To further validate and optimize on the basis of this structure, four geometries with varying distances between liquid channel front end and nozzle outlet were established. Such distance is denoted as the parameter *Len* shown in Fig. 1. The values of *Len* were 0.05, 0.1, 0.15, and 0.2 mm. The wall thickness between gas channel and liquid channel is denoted as the parameter *Wid* described in Fig. 1. The value of *Wid* was 20 μm. Figure 3b illustrates the axis static pressure distribution in the length of *Len*, and the nozzle outlet was at the 0 mm position. The four lines represented the pressures alone the axis from nozzle outlet to liquid channel front end in four geometries of *Len* respectively. The pressure at the end of each lines represented the pressure of liquid channel front end, thus, as shown in Fig. 3b, negative pressure was observed at the liquid channel front end in all four geometries. The lines in wave form might be caused by turbulence. Furthermore, when *Len* was

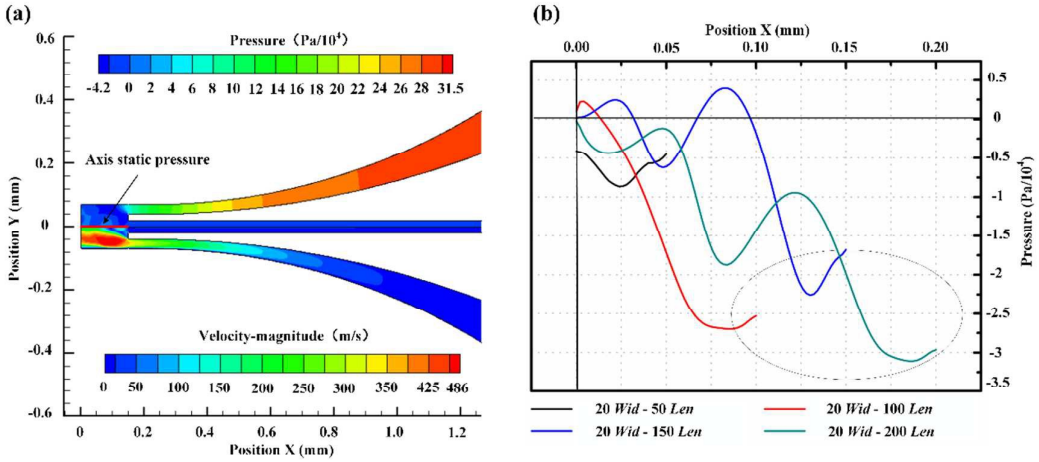

Fig. 3 Simulation results of the 20 µm wall thickness microfluidic chip. (a) Pressure (upper half) and velocity–magnitude (lower half) nephogram. (b) Negative pressure of the axis from the nozzle outlet to the liquid channel front end (red line in Fig. 3a). 20 *Wid*–50 *Len* means the wall thickness between gas channel and liquid channel (the parameter *Wid*) was 20 µm, and the distance between liquid channel front end and nozzle outlet (the parameter *Len*) was 50 µm.

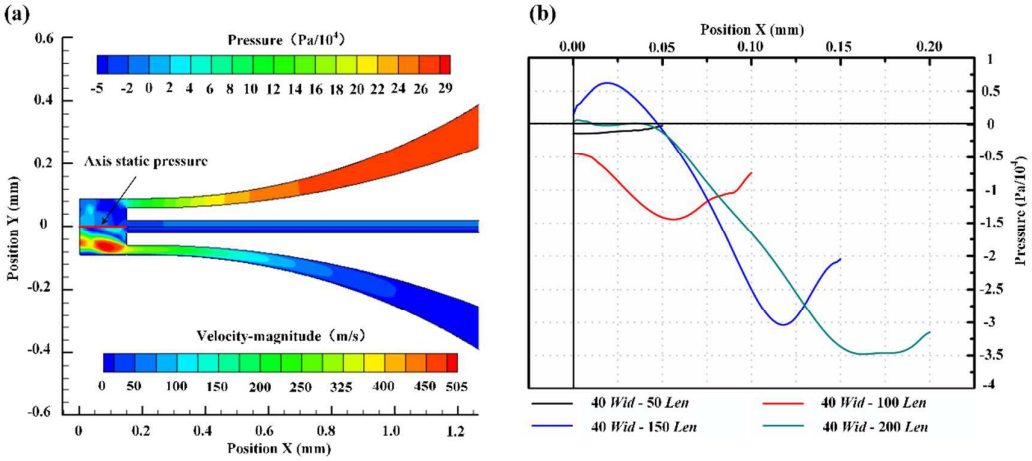

Fig. 4 Simulation results of the 40 µm wall thickness microfluidic chip. (a) Pressure (upper half) and velocity–magnitude (lower half) nephogram. (b) Negative pressure of the axis from the nozzle outlet to the liquid channel front end (red line in Fig. 4a). 40 *Wid*–50 *Len* means the wall thickness between gas channel and liquid channel (the parameter *Wid*) was 40 µm, and the distance between liquid channel front end and nozzle outlet (the parameter *Len*) was 50 µm.

0.05 mm, the absolute pressure value at the liquid channel front end was lower than the longer ones of *Len* as shown in the grey ellipse. In other words, when *Len* was 0.05 mm, much higher pressure at the gas inlet was required to obtain the comparable negative pressure at the liquid channel front end. The influence of wall thickness on the negative pressure was also considered. Another four different geometries were established. The values of *Len* were also 0.05, 0.1, 0.15, and 0.2 mm. However, the value of *Wid* was 40 µm. The simulation result is shown in Fig. 4. Because of the wider wall thickness, the turbulence had less influence on the axis, thus the more the liquid channel recessed inside, the lower the negative pressure was at the liquid channel front end.

Application of the Proposed Microfluidic Chip Coupled with MS

To ensure that the negative pressure was large enough to drive the liquid automatically and the wall thickness was thick enough to prevent the two PDMS slabs from being broken by high gas pressure, the geometry of 20 µm wall thickness was chosen in real fabrication. Moreover, if the liquid channel recessed inside more than 0.2 mm, liquid samples might flow attached the bottom wall in front of the liquid channel front end, which might affect spray stability. Thus, three geometries of *Len* with values of 0.05, 0.1, and 0.15 mm were selected to fabricate the microfluidic chips. Then, these chips were coupled with MS. The configuration of the microfluidic chip with the MS is illustrated in Fig. 5. The microfluidic chip was held by a laboratory-built platform and coupled with the ion-trap MS. The distance between the microfluidic chip emitter and the MS inlet orifice was nearly 4–10 mm. This distance was adjusted by a multi-dimensional manipulator.

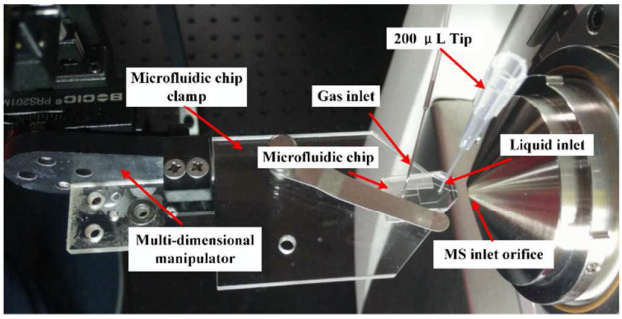

Fig. 5 Configuration of the microfluidic chip with the MS.

Figure 6 shows the MS signal of 83 µM reserpine in 3/1 (v/v) methanol/water with 0.2% formic acid. Helium was applied in the gas channel. The pressures of chip1 (100 µm *Len*), chip2 (50 µm *Len*), and chip3 (150 µm *Len*) were 0.34, 0.42, and 0.32 MPa, respectively, which were the optimum spray pressures for each chip. The flow rate of liquid samples was approximately 5 µL/min. Figure 6a shows the 5 min mean signal of reserpine

from chip1 and the base peak mean intensity was nearly 2.3 × 10^4. The signal stabilities of the three chips are displayed in Fig. 6b. As shown in the figure, the relative standard deviation for the total ion currents (TICs) of chip1, chip2, and chip3 were 4%, 5.19% and 3.5%, respectively. The mean TICs for chip1, chip2, and chip3 were 3.75 × 10^5, 2.77 × 10^5, and 2.95 × 10^5, respectively. Notably, chip1 had a slightly high TIC and chip3 had a slightly better stability. These results verified the stability of the proposed microfluidic chip.

To further study the influence of gas pressure on the negative pressure and the MS signal intensity, various pressures were applied on chip1, chip2, and chip3 to investigate the corresponding MS signal intensity. The pressure step was 0.5

MPa for each chip. Figure 7 illustrates the relationship between gas pressure and MS signal intensity. If the gas pressure was very low, then negative pressure might fail to drive the liquid samples. However, if the gas pressure was very high, then turbulence might prevent the liquid samples to spray out stably. Both conditions failed to provide any MS signal. As shown in

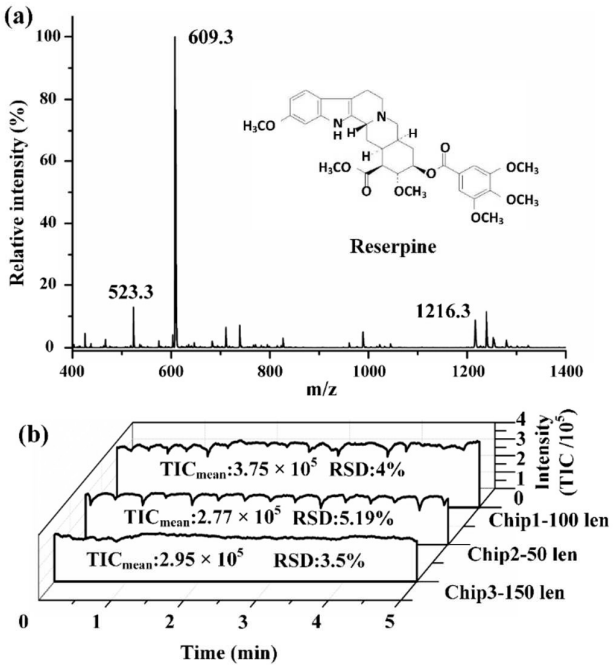

Fig. 6 MS signal of 83 µM reserpine in 3/1 (v/v) methanol/water with 0.2% formic acid; helium was applied in the gas channel. (a) Reserpine ion counts of the 5 min mean signal from chip1. (b) Reserpine signal stability of three chips for 5 min; optimum spray pressures of chip1, chip2, and chip3 were 0.34, 0.42, and 0.32 MPa, respectively. TICs mass range was from 605 to 614.

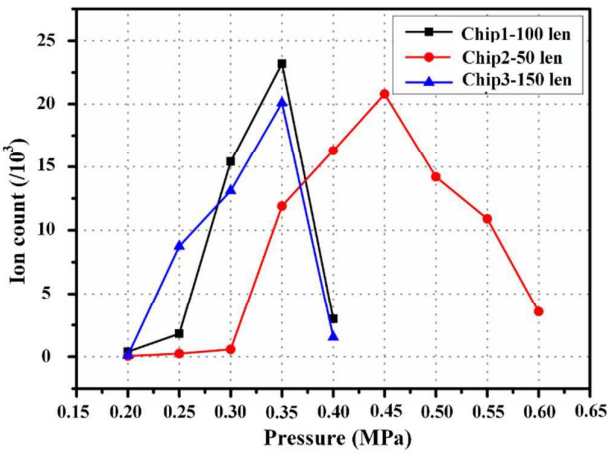

Fig. 7 Relationship between gas pressure and MS signal intensity of three chips. Helium was applied in the gas channel.

Fig. 7, the highest MS signal intensities of chip1 and chip3 were obtained all at 0.35 MPa, their optimum gas pressure for chip1 (0.34 MPa) and chip3 (0.32 MPa) were comparable. Comparatively, chip2 required much higher gas pressure (0.42 MPa) to obtain the highest MS signal intensity. As demonstrated in the simulation, a longer distance between nozzle outlet and liquid channel front end leads to a higher absolute value of negative pressure. In other words, chip2 required higher gas pressure than chip1 and chip3 to achieve a similar negative pressure. This finding is in accordance with the experimental results, as displayed in Fig. 7.

Experiments on other representative liquid samples, including trichlorphon, LTQ ESI positive ion calibration solution, and myoglobin, were also performed using chip1. Helium was also applied in the gas channel. Figure 8a displays the MS signal of 0.36 mM trichlorphon in 1/1 (v/v) methanol/water with 0.2% formic acid. Figure 8b shows the MS signal of LTQ ESI positive

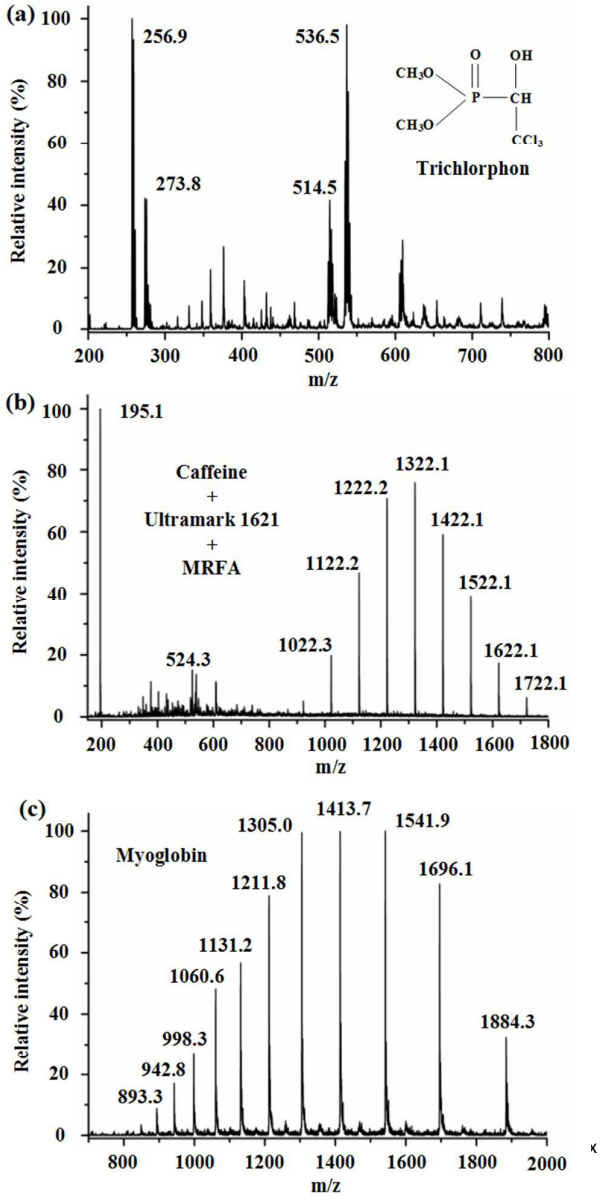

Fig. 8 MS signal of (a) 0.36 mM trichlorphon in 1/1 (v/v) methanol/water with 0.2% formic acid; (b) LTQ ESI positive ion calibration solution; (c) 200 μg mL-1 myoglobin in 1/1 (v/v) methanol/water.

ion calibration solution. This solution contains caffeine (200 ug), MRFA (10 ug), and Ultramark 1621 (0.001%) in a solution of 50% acetonitrile/25% methanol/24% water/1% acetic acid per 10 mL of solution. The protonated molecule of this solution was similar to the ESI MS signal. Figure 8c illustrates the MS signal of 200 μg mL-1 myoglobin in 1/1 (v/v) methanol/water. The performance of this biomolecule was similar to other SSI studies.[3, 42]

Furthermore, a few interesting phenomena were observed in different gases including helium, nitrogen, and argon. The MS signals of a home-made macro self-pumping SSI and the proposed microfluidic chip were compared. The home-made macro SSI was fabricated referring to other relative literatures.[3, 13] A fused-silica capillary (i.d. = 100 μm and o.d. = 400 μm) was coaxial with a stainless steel tube (i.d. = 500 μm and o.d. = 1 mm) and protruded out 0.5 mm at the stainless steel tube exit. Gas pressures on the macro SSI were all nearly 1.3 MPa. Liquid samples of reserpine, trichlorphon, and calibration solution were the same with the samples mentioned above. MS signals were all recorded at the optimum conditions at each

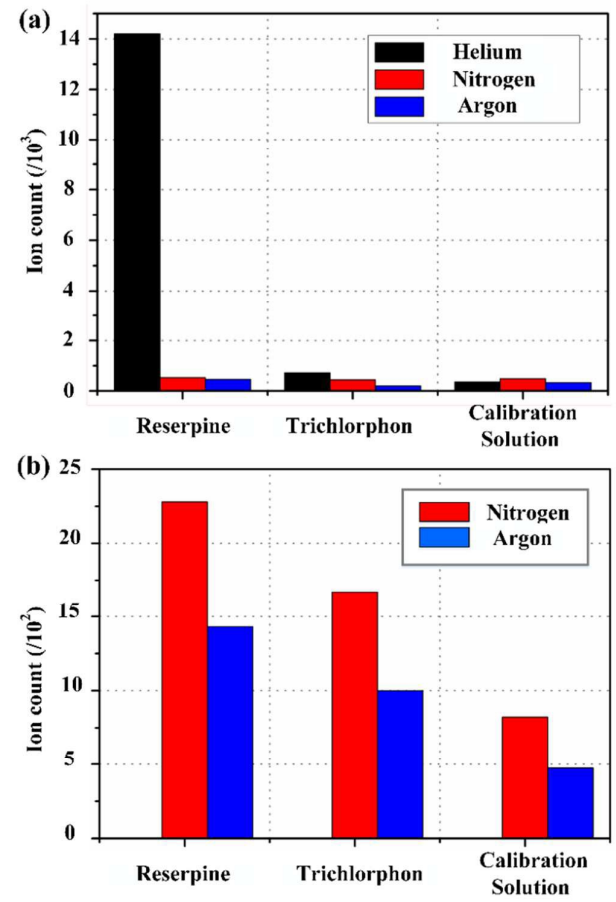

Fig. 9 MS signal of (a) microfluidic SSI chip; the gas pressure was around 0.35 MPa; helium, nitrogen, and argon were applied on the gas channel; (b) macro SSI chip; the gas pressure was nearly 1.3 MPa; nitrogen and argon were applied on the gas channel. Liquid samples were the same as those in Figs. 6 and 8.

experiment. The MS signal intensities of reserpine, trichlorphon, and calibration solution detected by the proposed microfluidic chip1 under different gases are shown in Fig. 9a. In general, the optimum gas pressure was around 0.35 MPa. Argon might require a slightly high gas pressure to achieve the optimum state. The signal intensity with helium was better than other gases, especially for reserpine; comparatively, experiments with argon obtained the lowest signal intensity. This finding is the same as the result of macro SSI as shown in Fig. 9b. In fact, ionization effect with various gases had been reported in the study of dielectric barrier discharge ion source[43], in which helium also obtained the best signal intensity. Apart from direct penning ionization, the internal energy of gas and other mechanism might also play significant roles.[7, 44, 45] Various samples likewise performed differently when 3-nitrobenzonitrile was added to improve sensitivity in SSI.[20] Further studies on the mechanism of SSI might also be needed.[13, 46] A comparison of the MS signal of the proposed microfluidic chip SSI and macro SSI indicated that the MS signal intensity of macro SSI was a little higher than micro SSI in total, except for reserpine; however, macro SSI required much higher gas pressure, which was a limitation of SSI desorption,[17] because the high pressure gas tend to blow away the solid samples. Moreover, when the high helium pressure was applied on the macro SSI, the vacuum of MS made the experiment impossible. In addition, comparing to macro ionization, microfluidic chip-based ionization also possessed many other advantages: integrating pre-treatment functions, implementing multi-channel ionization formation, and miniaturizing ionization size for portable MS.

Application of Dual-channel Microfluidic Self-aspiration SSI chip Coupled with MS

Internal calibration is an effective method in accurate mass measurement. The simplest form of internal calibration is to mix the reference and analyte together and then ionize the mixture simultaneously. However, ion suppression of the two compounds might prevent this method from being used widely. Dual sprayers, one of which sprays the analyte and the other the reference compound, can effectively reduce such ion suppression.[47] Ramsey *et al.*[35] have reported a microfluidic chip based dual-sprayers. However, because of the severe interference among the electric fields of the adjacent sprayers, this method failed to generate signals of the analyte and the reference compounds simultaneously.

As an extended application of the proposed microfluidic self-aspiration SSI chip, dual-channel microfluidic self-aspiration SSI chip was fabricated. Because the wall thickness might become narrow in real fabrication, especially when the channel is deep. Therefore, we designed the wall thickness *Wid* as 40 μm. This dual-channel SSI chip implemented self-aspiration of the

analyte and the reference compound simultaneously without high voltage. The spray effect is shown in Fig. 10. Despite the spraying out of the microfluidic chip was only observed as one bright spot, as shown in Fig. 10a, the two spray tips were generated in the liquid channel front ends separately, as shown in the red ellipses in Fig. 10b. This spray form helps to reduce

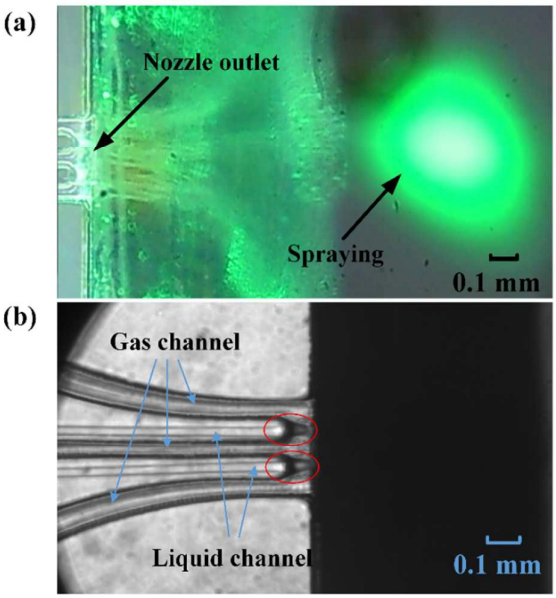

Fig. 10 Spray effect of (a) in and (b) out of the dual-channel microfluidic self-aspiration SSI chip. The total gas pressure on gas channel inlet was 0.4 MPa. Two spray tips were shown in red ellipses.

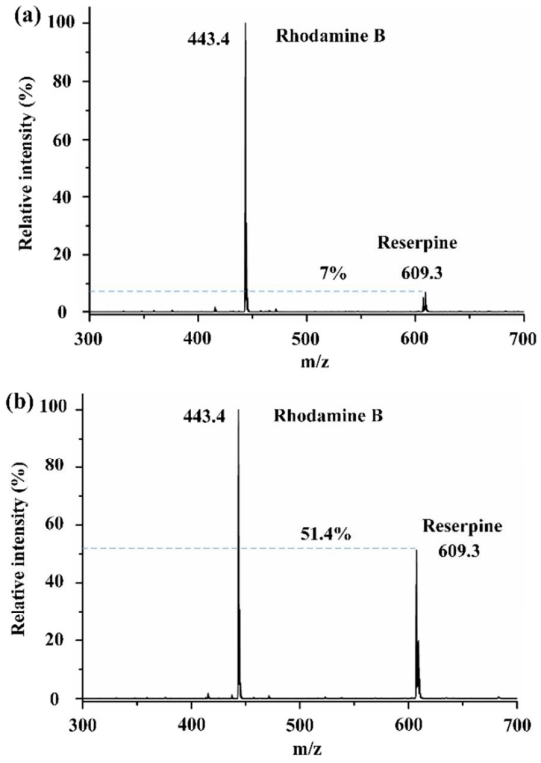

Fig. 11 MS signal of (a) single channel sprayed with mixture solution of reserpine and rhodamine B (TIC 700); (b) dual-channel sprayed with reserpine and rhodamine B solution separately (TIC 1520). Reserpine solution was 41 µM in 3/1 (v/v) methanol/water with 0.2% formic acid and rhodamine B was 50 µM in 1/1 (v/v) methanol/water with 0.2% formic acid.

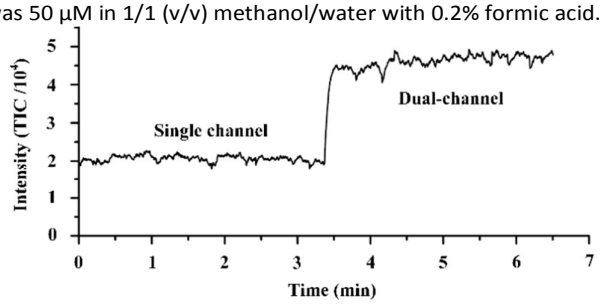

Fig. 12 TIC intensity of 41 µM reserpine in 3/1 (v/v) methanol/water with 0.2% formic acid. In the first 3.5 minute, reserpine was sprayed by only one channel; in the last 3 minute, two channels sprayed reserpine simultaneously. The total gas pressure was about 0.4 MPa.

the ion suppression greatly. Fig. 11 demonstrates the ion suppression effect. The intensity of reserpine was only 7% of rhodamine B when these two solutions were mixed together and sprayed by only one liquid channel. However, the intensity of reserpine increased to 51.4% of rhodamine B when these two solutions were sprayed by the dual-channel separately. As shown in Fig. 11, the ion suppression was reduced greatly. Furthermore, the TICs intensities of reserpine sprayed by single channel and dual-channel were compared. In the first 3.5 minutes, we only added reserpine solution in one 200 µL tip of the dual-channel SSI chip, then the reserpine solution was also added in another 200 µL tip in the last 3 minutes without any alteration. Fig. 12 shows that the signal intensity was enhanced about two times when using the dual-channel sprayed simultaneously. Further application study of the dual-channel microfluidic self-aspiration SSI chip will be performed later. It might be the simplest ionization source to implemented internal calibration for MS in the future.

Conclusion

A novel microfluidic self-aspiration SSI chip was developed to ionize liquid samples under ambient conditions. Three-layer soft lithography technology was used to fabricate this ionization chip. The proposed ionization chip avoided the problems of manufacturing the spraying tips and prevented the universal disadvantages, such as liquid spreading and dead volume of the microfluidic chips coupled with MS. Moreover, the proposed ionization chip successfully introduced the gas channel, implemented self-aspiration with much lower gas pressure than macro SSI, and realized sample ionization without high voltage. Dual-channel self-aspiration sonic-spray ionization chip was proved to reduce the ion suppression, which was important in internal calibration. These advantages

might make significant contributions to promoting the development of corresponding pre-treatment function integration and parallel on-chip ionization for miniaturized MS in our future works.

Acknowledgments

This work is supported by the National Natural Science Foundation of China (Grant No. 81201165) and Shenzhen fundamental research funding (Grant No. JCYJ20140902110354240 and No. JC201005280634A).

References

1. Z. Ouyang and R. G. Cooks, *Annu. Rev. Anal. Chem.*, 2009, **2**, 187-214.
2. H. Gang, C. Yi, T. Fei, L. Li-Tao and W. Xiaohao, *AIP. ADV.*, 2015, **5**, 041303.
3. V. G. Santos, T. Regiani, F. F. G. Dias, W. Romao, J. L. P. Jara, C. F. Klitzke, F. Coelho and M. N. Eberlins, *Anal. Chem.*, 2011, **83**, 1375-1380.
4. J. B. FENN, M. MANN, C. K. MENG, S. F. WONG and C. M. WHITEHOUSE, *SCIENCE*, 1989, **246**, 64-71.
5. Z. Takats, J. M. Wiseman, B. Gologan and R. G. Cooks, *SCIENCE*, 2004, **306**, 471-473.
6. R. B. Cody, J. A. Laramee and H. D. Durst, *Anal. Chem.*, 2005, **77**, 2297-2302.
7. J. D. Harper, N. A. Charipar, C. C. Mulligan, X. Zhang, R. G. Cooks and Z. Ouyang, *Anal. Chem.*, 2008, **80**, 9097-9104.
8. R. Haddad, H. Milagre, R. R. Catharino and M. N. Eberlin, *Anal. Chem.*, 2008, **80**, 2744-2750.
9. T. R. Covey, B. A. Thomson and B. B. Schneider, *Mass Spectrom. Rev.*, 2009, **28**, 870-897.
10. A. HIRABAYASHI, M. SAKAIRI and H. KOIZUMI, *Anal. Chem.*, 1994, **66**, 4557-4559.
11. J. M. Wiseman, Z. N. Tak Ts, B. Gologan, V. J. Davisson and R. G. Cooks, *Angew. Chem. Int. Ed.*, 2005, **44**, 913-916.
12. Z. Takats, J. M. Wiseman, B. Gologan and R. G. Cooks, *Anal. Chem.*, 2004, **76**, 4050-4058.
13. Z. Takats, S. C. Nanita, R. G. Cooks, G. Schlosser and K. Vekey, *Anal. Chem.*, 2003, **75**, 1514-1523.
14. E. M. Borges, D. A. Volmer and M. N. Eberlin, *Can. J. Chem.*, 2013, **91**, 671-678.
15. R. Haddad, R. Sparrapan and M. N. Eberlin, *Rapid Commun. Mass Spectrom.*, 2006, **20**, 2901-2905.
16. Y. E. Corilo, B. G. Vaz, R. C. Simas, H. D. Lopes Nascimento, C. F. Klitzke, R. C. L. Pereira, W. L. Bastos, E. V. Santos Neto, R. P. Rodgers and M. N. Eberlin, *Anal. Chem.*, 2010, **82**, 3990-3996.
17. R. M. Alberici, R. C. Simas, V. de Souza, G. F. de Sa, R. J. Daroda and M. N. Eberlin, *Anal. Chim. Acta*, 2010, **659**, 15-22.
18. S. A. Saraiva, P. V. Abdeinur, R. R. Catharino, G. Nunes, M. N. Eberlin, L. S. Eberlin, P. V. Abdelnur, A. Passero, G. F. de Sa, R. J. Daroda, V. de Souza and M. N. Eberlin, *Rapid Commun. Mass Spectrom.*, 2009, **23**, 357-362.
19. R. Haddad, R. R. Catharino, L. A. Marques and M. N. Eberlin, *Rapid Commun. Mass Spectrom.*, 2008, **22**, 3662-3666.
20. K. Kanaki and S. A. Pergantis, *Rapid Commun. Mass Spectrom.*, 2014, **28**, 2661-2669.
21. G. Li and G. Huang, *J. Mass Spectrom.*, 2014, **49**, 639-645.
22. D. Gao, H. X. Liu, Y. Y. Jiang and J. M. Lin, *Lab. Chip.*, 2013, **13**, 3309-3322.
23. S.-L. Lin, H.-Y. Bai, T.-Y. Lin and M.-R. Fuh, *ELECTROPHORESIS*, 2012, **33**, 635-643.
24. S. Koster and E. Verpoorte, *Lab Chip*, 2007, **7**, 1394-1412.
25. W. C. Sung, H. Makamba and S. H. Chen, *ELECTROPHORESIS*, 2005, **26**, 1783-1791.
26. Q. F. Xue, F. Foret, Y. M. Dunayevskiy, P. M. Zavracky, N. E. McGruer and B. L. Karger, *Anal. Chem.*, 1997, **69**, 426-430.
27. R. S. Ramsey and J. M. Ramsey, *Anal. Chem.*, 1997, **69**, 1174-1178.
28. J. Li, P. Thibault, N. H. Bings, C. D. Skinner, C. Wang, C. Colyer and J. Harrison, *Anal. Chem.*, 1999, **71**, 3036-3045.
29. X. Sun, R. T. Kelly, K. Tang and R. D. Smith, *ANALYST*, 2010, **135**, 2296-2302.
30. P. Mao, R. Gomez-Sjoberg and D. Wang, *Anal. Chem.*, 2013, **85**, 816-819.
31. P. Mao, H.-T. Wang, P. Yang and D. Wang, *Anal. Chem.*, 2011, **83**, 6082-6089.
32. X. Qian, J. Xu, C. Yu, Y. Chen, Q. Yu, K. Ni, X. Wang, D. Gao, H. X. Liu, Y. Y. Jiang and J. M. Lin, *SENSORS*, 2015, **15**, 8931-8944.
33. J.-B. Hu, T.-R. Chen, C.-H. Chang, J.-Y. Cheng, Y.-C. Chen and P. L. Urban, *The Analyst*, 2015, **140**, 1495-1501.
34. C. Yu, X. Qian, Y. Chen, Q. Yu, K. Ni and X. Wang, *Micromachines*, 2015, **6**, 1890-1902.
35. A. G. Chambers and J. M. Ramsey, *Anal. Chem.*, 2012, **84**, 1446-1451.
36. M. Trebbin, K. Krüger, D. DePonte, S. V. Roth, H. N. Chapman and S. Förster, *Lab. Chip.*, 2014, **14**, 1733.
37. M. A. Unger, H. P. Chou, T. Thorsen, A. Scherer and S. R. Quake, *SCIENCE*, 2000, **288**, 113-116.
38. Y. Œ. W. G. Xia, *Angew. Chem. Int. Ed.*, 1998, **37**, 550 - 575.
39. P. Jurčíček, L. Liu and H. Zou, *Int. J. Ion. Mobil. Spectrom.*, 2014, **17**, 157-166.
40. P. Jurčíček, H. Zou and S. Gao, *J. Micro-Nanolith. Mem.*, 2013, **12**, 023006-023006.
41. G. Jarvas, J. Grym, F. Foret and A. Guttman, *Electrophoresis*, 2015, **36**, 386-392.
42. M. M. Antonakis, A. Tsirigotaki, K. Kanaki, C. J. Milios and S. A. Pergantis, *J. Am. Soc. Mass. Spectrom.*, 2013, **24**, 1250-1259.
43. C. Guo, F. Tang, J. Chen, X. Wang, S. Zhang and X. Zhang, *Anal. Bioanal. Chem.*, 2015, **407**, 2345.
44. R. B. Cody, J. A. Laramée and H. D. Durst, *Anal. Chem.*, 2005, **77**, 2297-2302.
45. N. Na, M. Zhao, S. Zhang, C. Yang and X. Zhang, *J. Am. Soc. Mass. Spectrom.*, 2007, **18**, 1859-1862.
46. D. Touboul, M. C. Jecklin and R. Zenobi, *Rapid Commun. Mass Spectrom.*, 2008, **22**, 1062-1068.
47. Y. Li, N. Zhang, Y. Zhou, J. Wang, Y. Zhang, J. Wang, C. Xiong, S. Chen and Z. Nie, *J. Am. Soc. Mass. Spectrom.*, 2013, **24**, 1446-1449.